Applied mechanics in grinding. Part 7: residual stresses induced by the full coupling of mechanical deformation, thermal deformation and phase transformation

Mofid Mahdi, Liangchi Zhang[*]

Department of Mechanical and Mechatronic Engineering, The University of Sydney, Sydney, NSW 2006, Australia

Abstract

In this final part of the series research on residual stresses in ground components, the full coupling of mechanical deformation, thermal deformation and phase transformation during grinding was investigated using the finite element method. It was found that all the components of surface residual stresses become tensile when phase transformation takes place. This phenomenon is independent of the cooling conditions and type of grinding operations and is affected only slightly by the variation of surface mechanical traction. The distribution of the residual stress in grinding direction is nearly linear in both the martensite and non-martensite zones. However, the location of the maximum residual stress is related to the surface mechanical traction and depth of martensite transformation. © 1999 Elsevier Science Ltd. All rights reserved.

Keywords: Residual stresses; Grinding; Mechanical deformation; Thermal deformation; Phase transformation; Full coupling

Nomenclature

D	constitutive matrix
d	martensite depth
e	error
H	non-dimensional heat transfer coefficient $(2\alpha h/\kappa v)$
h	heat transfer coefficient of coolant
L_c	length of grinding zone, see Fig. 1

* Corresponding author. Tel.: + 0061-2-9351-2835; fax: + 0061-2-9351-3760; e-mail: zhang@mech.eng.usy-d.edu.au

l_a	relative peak location of a heat flux ($2\zeta_a/L_c$), where ζ_a is defined in Fig. 1
M	Martensite
Pe	Peclet number ($vL_c/4\alpha$)
p	traction pressure, see Fig. 1
p_a	peak value of the traction pressure
q	heat flux per unit grinding width, see Fig. 1
q_a	peak value of the heat flux
T	temperature rise with respect to ambient temperature, T_∞
v	moving speed of the heat source, see Fig. 1
w	cooling factor, defined in Eq. (1)
Y	yield stress of the work material
α	thermal diffusivity
κ	thermal conductivity of work material
μ	ratio of horizontal to vertical traction
ν	Poisson's ratio
σ	stress tensor

Subscripts

aust	austenizing
max	maximum
T	thermal
x,y,z	x-, y-, and z-directions, see Fig. 1
y	yield
∞	room temperature

1. Introduction

For a workpiece subjected to grinding, mechanical plastic deformation, thermal plastic deformation and irreversible deformation due to phase transformation are the major causes of residual stress generation [1]. In the previous parts of our series of studies, we have developed an adaptive numerical approach to handle the analyses of grinding temperature and phase transformation [2–4], residual stresses caused by surface mechanical loading [5], thermal plastic deformation [6], coupling of thermal plastic deformation and phase transformation [7] and the combination of mechanical and thermal plastic deformation [8]. Our research showed that residual stress distribution is sensitive to the combination of grinding-induced permanent deformation and that the change of causes of deformation may change the nature of residual stresses completely.

Under certain grinding conditions, plastic deformation by mechanical and thermal loading and the irreversible deformation due to phase transformation may occur simultaneously in some specific work materials. The distribution of residual stresses in those ground components, therefore, may vary in a different manner. This study aims to understand the full coupling effect of all the sources on the variation of residual stresses.

2. Modelling

2.1. Mechanics and algorithm

As discussed previously [2–8], the deformation in a workpiece subjected to surface grinding can be considered as a plane-strain problem, and the heat flux generated by grinding can be approximated by a triangular heat source, moving along the positive direction of *x*-axis on the workpiece surface, as shown in Fig. 1. The surface mechanical stress due to grinding can also be simulated by a moving triangular traction with its peak being coincident with that of the heat flux. In this way, the mechanical cutting of the grinding wheel in the finite element analysis can be simulated by equivalent nodal forces. The direction of the horizontal nodal forces depends on the type of grinding processes, being positive for an up-grinding and negative for a down-grinding. Meanwhile, the type of grinding processes also alters the height (p_a or q_a) and location (l_a) of the peaks of the surface mechanical traction and heat flux, respectively, as shown in Fig. 1.

The cooling effect of grinding fluid can be modelled by a variable coefficient of convection heat transfer, that is.

$$q_c = hT, \quad |2x/L_c| \geq 1$$
$$q_c = whT, \quad |2x/L_c| < 1 \tag{1}$$

where q_c is the convection heat flux, w is an effective cooling factor over the workpiece surface, with $w = 1$ indicating a uniform convection over the whole workpiece surface, $0 \leq w < 1$ representing a less effective cooling, and $w > 1$ standing for a super-cooling inside the grinding zone.

To account for the property change of work materials by phase transformation, the special constitutive model developed in our previous study [7] is coded and realised by the user-supplied routine function in ADINA [9]. A subroutine is then developed to express the constitutive matrix of an elastic–plastic work material and to update stresses using the Newton–Raphson method
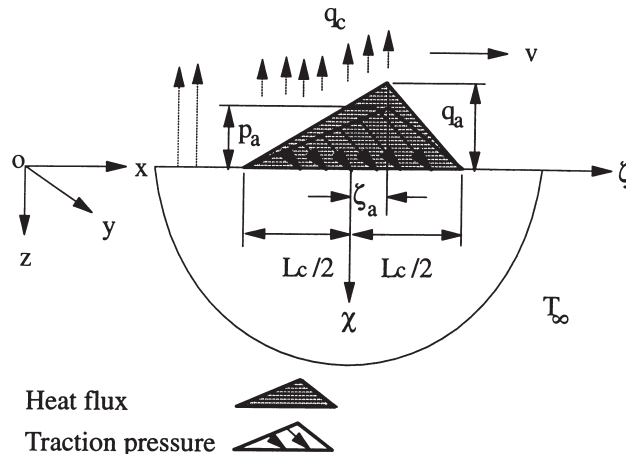

Fig. 1.   A theoretical model of surface grinding with convection.

[10]. Fig. 2 shows the detailed updating structure of grinding stresses of the above algorithm that fully couples the mechanical deformation, thermal deformation and the irreversible deformation induced by phase transformation. To compare the residual stresses with those due to individual causes, such as sole thermal deformation or sole phase transformation investigated previously, the present study still uses EN23 steel as the workpiece material, whose properties and compositions can be found elsewhere [2–8].

Compared with the dimension of a grinding zone, a workpiece should be considered as a semi-

Start

Initialize the stress and strain fields

Calculate the strain increments, $\Delta\varepsilon$, based on displacement increments

Calculate the stress increments, $\Delta\sigma$, by assuming elastic behavior with elastic stiffness matrix, D_e, ie $\Delta\sigma_e = D_e\Delta\varepsilon$

Update the new trial stress $\sigma_t = \sigma_i + \Delta\sigma$

Yielding $F(\sigma_t) > Y(T)$? — N / Y

Replace the trial stress, σ_t, as the initial stress, σ_i, for next solution increment as $\sigma_i = \sigma_t$

Find the ratio of elastic stress increment, r, prior to yielding by solving $F(\sigma_i + r\ \Delta\sigma) = 0$ and evaluate the elastic stress increments, $\Delta\sigma_e$ based on the new ratio, r, and the elastic-stiffness matrix, D_e, ie $\Delta\sigma_e = (D_e r)\Delta\varepsilon$

Initialize counter n and total plastic stress increments, $\Delta\sigma_p^t$, ie $n = 0$ and $\Delta\sigma_p^t = 0$

$n = n+1$

Calculate the plastic stress sub-increments, $\Delta\sigma_p$, based on the new ratio, r, the total number of subdivisions, n_{max}, and the elastic-plastic stiffness matrix, D_{ep} (σ), ie $\Delta\sigma_p = D_{ep} (1-r)\Delta\varepsilon/n_{max}$

Update the total plastic stress sub-increments, $\Delta\sigma_p^t$, ie $\Delta\sigma_p^t = \Delta\sigma_p^t + \Delta\sigma_p$

$n = n_{max}$? — N / Y

Update the initial stress, σ_i, of the next solution step, ie $\sigma_i = \sigma_i + \Delta\sigma_e + \Delta\sigma_p^t$

Update the new geometry and boundary conditions

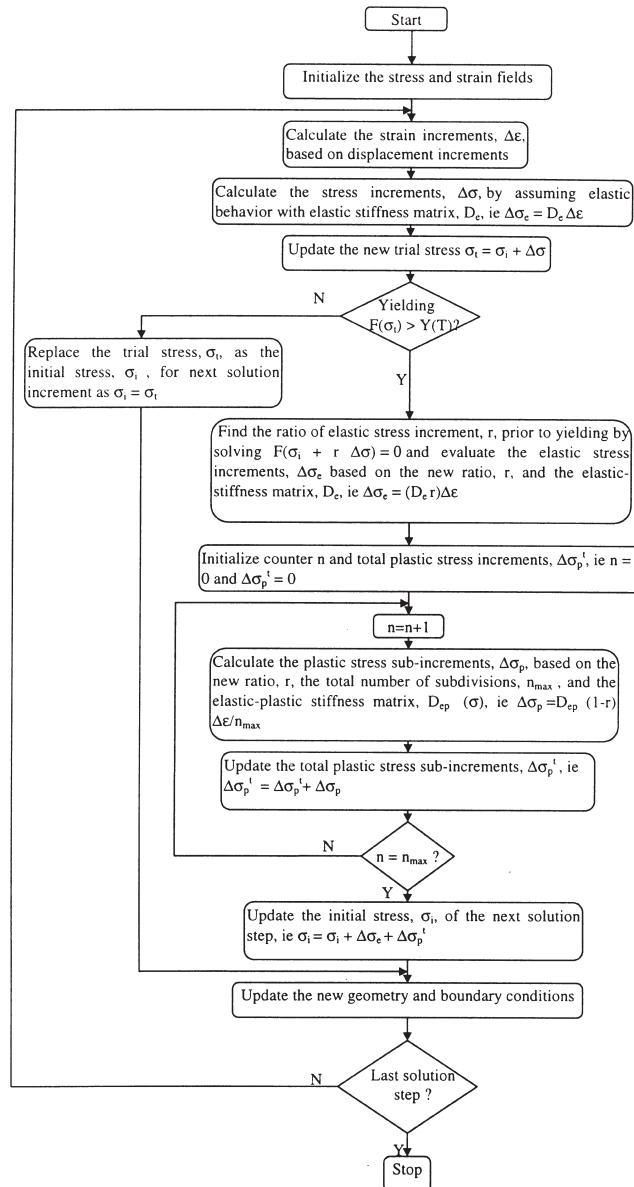Last solution step? — N / Y

Stop

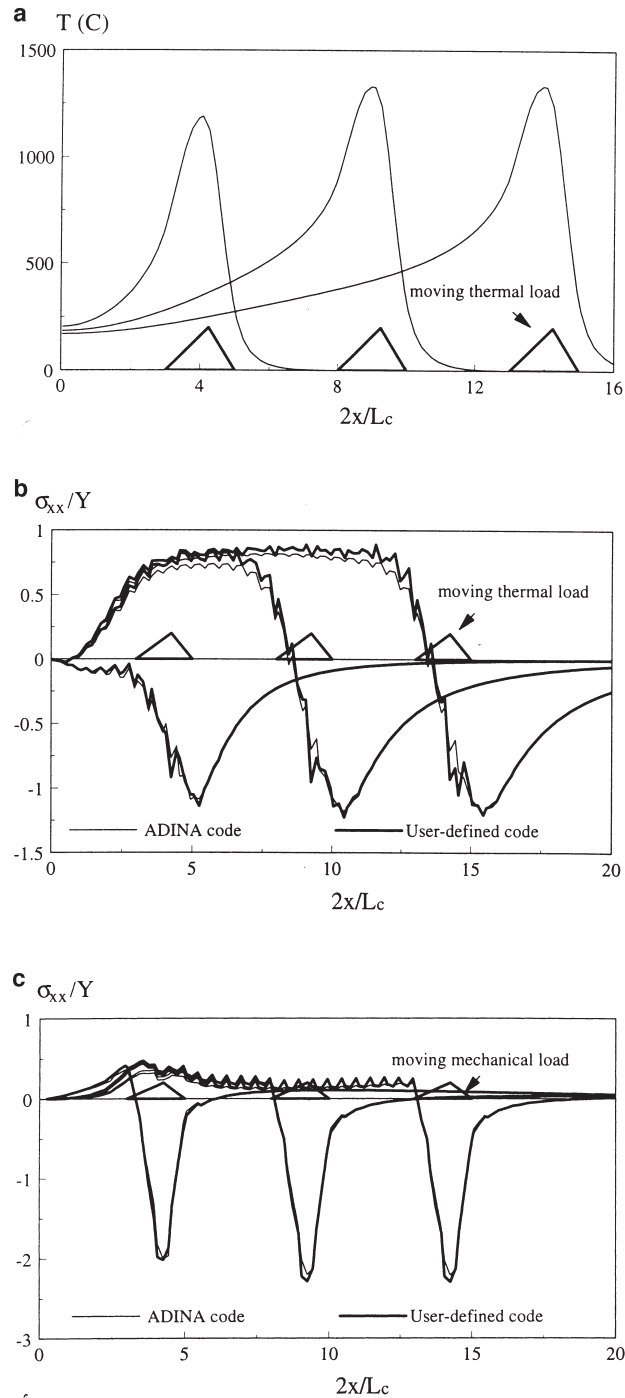Fig. 2.   An algorithm of explicit stress integration.

Fig. 3.   A typical up-grinding analysis with transient thermal and mechanical deformation (no sub-division for stress increments; constant material properties; $l_a = 0.25$). (a) Surface temperature generated by grinding ($H = 0$, Pe = 1 and $q_a = 80$ MW/m²). (b) Longitudinal thermal stress, σ_{xx} ($p_a = 0$, $H = 0$, Pe = 1 and $q_a = 80$ MW/m²). (c) Longitudinal mechanical stress, σ_{xx} ($p_a = 2Y$, $\mu = 0.1$, $q_a = 0$).

infinite body.[1] Thus, to eliminate the boundary effect due to mechanical and thermal loading, a large control volume in the finite element analysis is necessary. In this study a dimension of $24L_c$ $\times$ $24L_c$ is used, which is 1.5 times bigger than that used in [7]. For simulating possible phase transformation, the surface layer with a thickness of $0.5L_c$ is divided into eight sub-layers using nine-node elements to provide a smooth transition of property changes of the work material. The whole control volume is divided by a total of 1248 nine-node quadratic elements with 5211 nodes.

For a reliable residual stress prediction, stress variation at a point after the action of surface traction and heat flux must be monitored until the real steady state is achieved. To this end, we use 80 solution steps after the action of the mechanical forces and heat flux, plus additional 20 steps to approximate the complete cooling and unloading by linearly drawing the grinding-induced temperature rise back to zero.

2.2. Accuracy of the numerical analysis

To verify the accuracy of the numerical analysis using the above user-supplied modelling technique, three special cases were examined against the standard elastic–plastic material model in ADINA with constant material properties. They are (1) thermal grinding conditions only, (2) grinding conditions with iso-thermal-mechanical conditions, and (3) a combination of cases (1) and (2). Fig. 3(a,b) illustrates the grinding temperature history and the corresponding thermal surface stresses in relation to the movement of heat flux under the condition of case (1). Fig. 3(c) shows the mechanical stress history in relation to the movement of the mechanical traction. It is clear that surface stresses reach their steady state after a few steps of heat flux movement. Thus, in terms of accuracy and stability, the history of thermal and mechanical surface stresses calculated by the user-defined code is in close agreement with those from the standard ADINA. Since the present stress updating algorithm is explicit and conditionally stable, as demonstrated by Fig. 2,
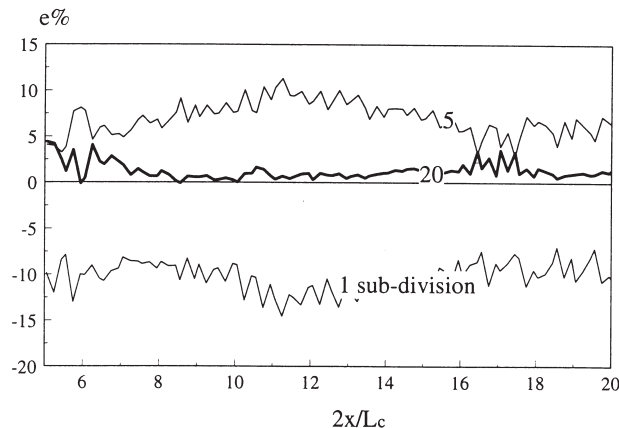

Fig. 4.   A typical stability analysis under thermo-mechanical grinding conditions ($H = 0$, $l_a = 0.25$, Pe $= 1$, $q_a = 80$ MW/m^2, $p_a = 2Y$, and $\mu = 0.1$).

---

[1] The grinding of thin plates is not the objective of this research, where the workpiece thickness is comparable with the grinding zone dimension.

the above case studies indicate that the effect of subdivision of stress increment in building up a smoother constitutive matrix must be considered carefully. The analysis of case (3) shows that more divisions of stress sub-increments in stress integration lead to closer results to those of ADINA. Fig. 4 demonstrates that 20 sub-increments bring about a relative error of less than 4%, which is acceptable in practice and therefore is used throughout the present study.

3. Results and discussion

When a workpiece experiences the critical temperature variation in grinding, phase change occurs at a certain distance away from the grinding zone, as demonstrated by Fig. 5. It is clear that phase change starts earlier if the coefficient of convection heat transfer, H, is higher, regardless of the variation of table speed, which is reflected by the change of the Peclet number, Pe. Moreover,
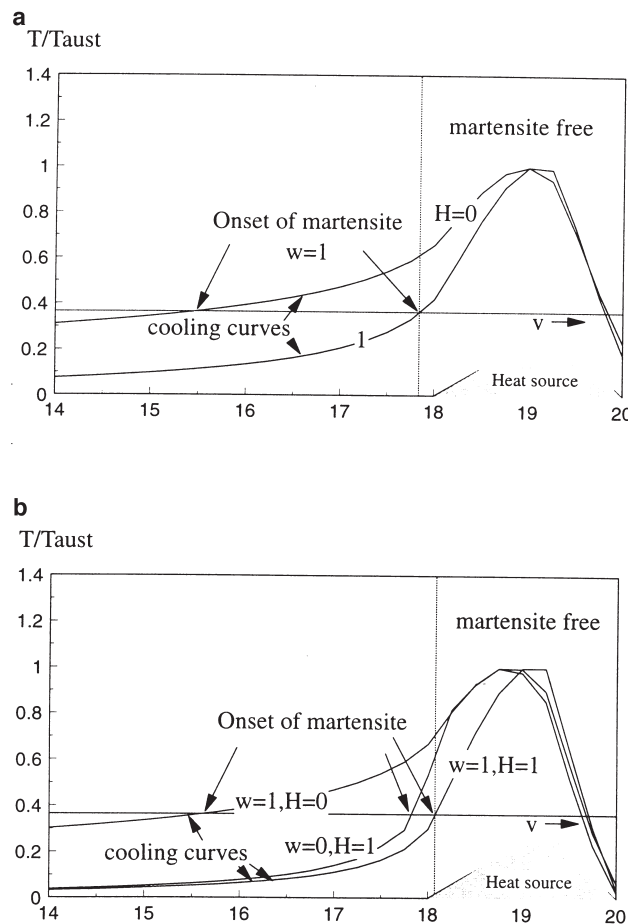
Fig. 5.   Onset of phase change versus heat source location; (a) Pe = 1 and l_a = 0.25, (b) Pe = 4 and l_a = 0.25.

a σ_{xx}/Y

b σ_{yy}/Y

c σ_{yy}/Y
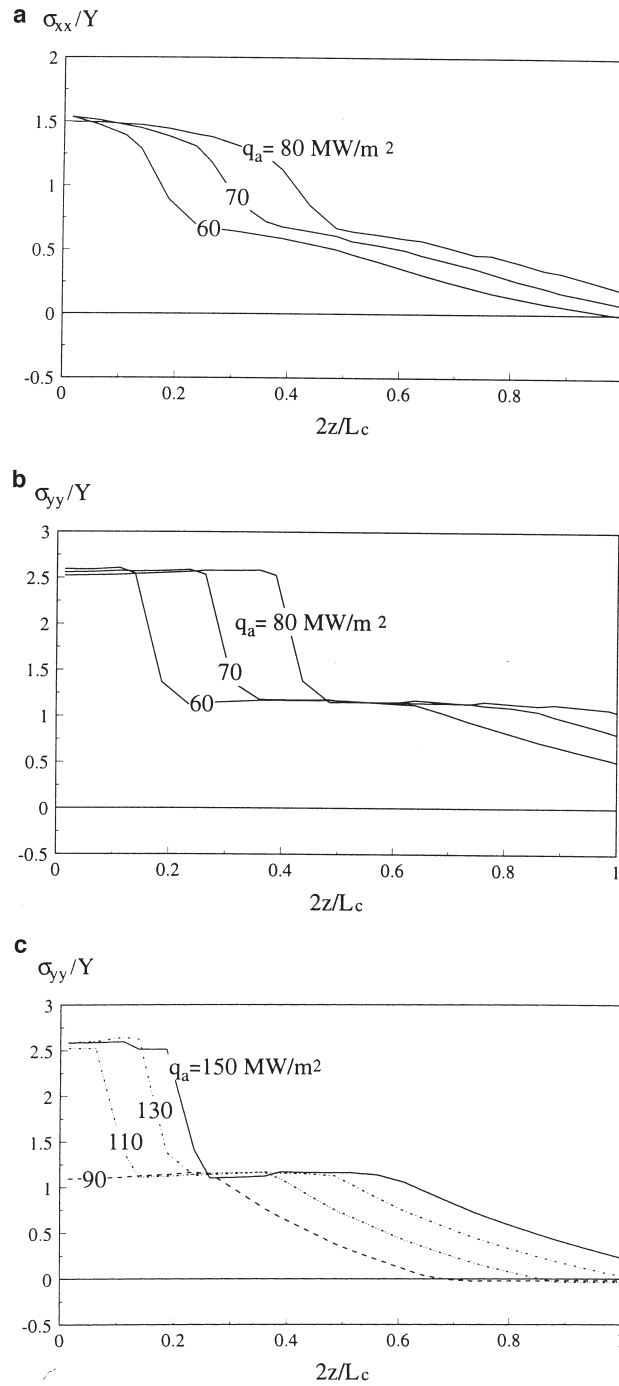
Fig. 6. Thermal residual stresses without surface cooling ($H = 0$, $l_a = 0.25$); (a) σ_{xx} with Pe = 1, (b) σ_{yy} with Pe = 1, (c) σ_{yy} with Pe = 4.

less cooling in the grinding zone ($0 \leq w < 1$) accelerates the initiation of phase transformation if H is high, for instance, $H = 1$.

The variation of grinding conditions does not affect the two major surface residual stresses, σ_{xx} and σ_{yy}, when phase transformation occurs, as shown in Fig. 6. The residual stress σ_{yy} is nearly constant across the martensite zone (Fig. 6(b,c)). The longitudinal residual stress σ_{xx}, however, changes linearly, with a limit, within the martensite zone. At the boundary of the martensite zone, a rapid change of residual stresses occurs due to the sudden change of workpiece properties. Compared with σ_{yy}, σ_{xx} is more affected by the types of grinding operations, the ratio of horizontal to vertical forces and the fully coupled thermo-mechanical grinding conditions with phase change. The maximum σ_{xx} and σ_{yy} are 1.5 and 2.6 times higher, respectively, than the initial yield stress of the workpiece, Y, and they are tensile at the ground surface. These characteristics are similar to those of purely thermal residual stresses without phase change as discussed in our previous
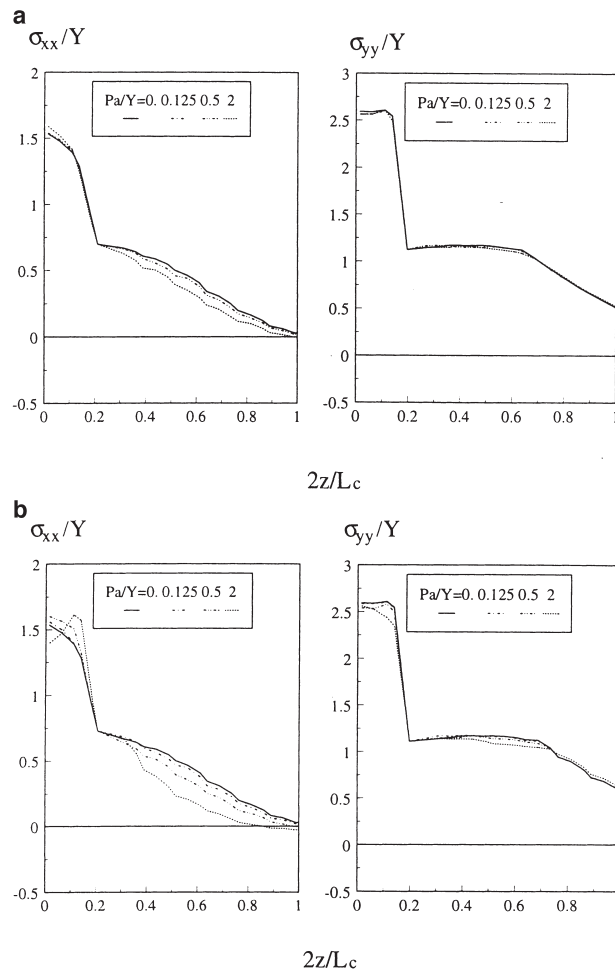

Fig. 7. The effect of mechanical traction on residual stresses ($H = 0$, $l_a = 0.25$, Pe $= 1$ and $q_a = 60$ MW/m^2); (a) $\mu = 0.1$, (b) $\mu = 0.3$.

study [6]. However, the coupling of phase transformation with thermal and mechanical deformation brings about much higher tensile residual stresses at the workpiece surface.

The coupling of mechanical loading with thermal loading and phase transformation has a minor influence on residual stress distribution for a wide range of magnitude of surface traction, as shown in Fig. 7. Moreover, at a higher ratio of horizontal to vertical traction, e.g. $\mu = 0.3$ (Fig. 7(b)), the increase of traction slightly decreases the longitudinal surface residual stress, σ_{xx}. The reason for that is related to the reduction of the longitudinal strain within the grinding zone. As shown in our previous investigation [5], a higher mechanical traction with a down-grinding produces less longitudinal tensile residual stresses. However, associated with the high mechanical traction, thermal strains become considerably higher and strains due to phase transformation also contribute remarkably to the workpiece deformation. Thus, compared with thermal deformation and phase transformation, the effect of mechanical traction becomes minor. In the case with martensite phase transformation, the strains at the austenizing grinding temperature play a central role in the formation of tensile residual stresses.
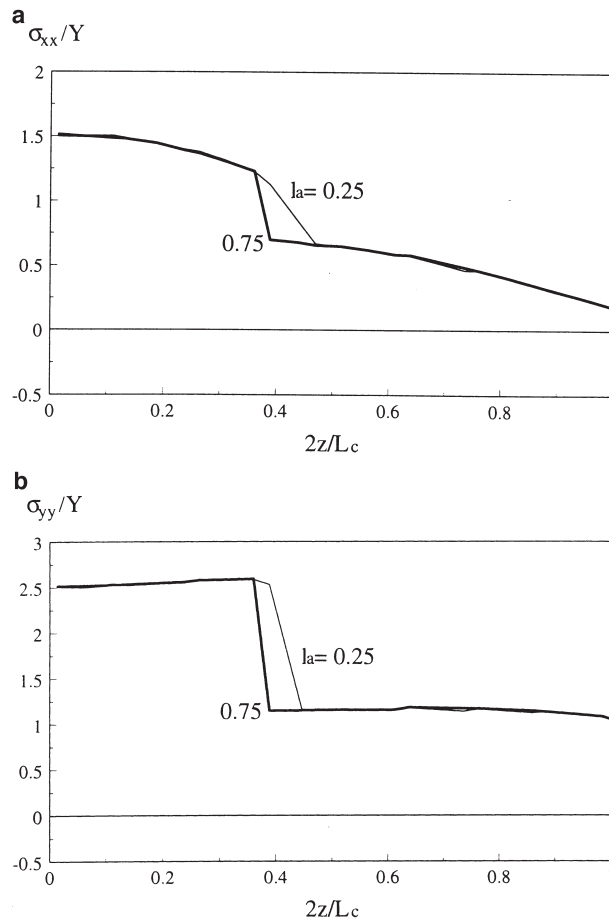

Fig. 8.   The effect of grinding type on residual stresses ($H = 0$, Pe $= 1$, $p_a = 0$ and $q_a = 80$ MW/m²); (a) σ_{xx}, (b) σ_{yy}.

An up-grinding (e.g. $l_a = 0.25$) results in a slightly thicker hardened layer, as shown in Fig. 8. This is reasonable because an up-grinding operation produces a higher grinding temperature if the other conditions are the same as in a down-grinding (e.g. $l_a = 0.75$). Furthermore, the depth of the zone with large residual stresses is directly related to the thickness of the hardened martensite layer that is characterised by a higher martensite yield stress, $(\sigma_y)_m$, about 2.8 times the original yield stress, Y, of the work material, as illustrated in Fig. 9. It is interesting to note that although the hardened layer thickness decreases as the input of grinding heat flux decreases, the level of maximum residual stresses in the martensite zone does not change. For a down-grinding process, similar dependence of residual stresses on the depth of the martensite zone exists.

The Peclet number of a grinding process, Pe, reflects the variation of the grinding table speed and thus the thermal energy diffusion rate through the ground surface. An increase of Pe results in a decrease of grinding temperature and an increase of cooling rate, if all the other grinding conditions are the same. Therefore, to maintain the same grinding temperature and martensite depth, a higher input of heat flux is needed compared with the cases of Fig. 9. Fig. 10 demonstrates the power of cooling mechanism on residual stress distributions. It is clear that no-cooling inside the grinding zone (i.e. $w = 0$) would decrease greatly the required heat flux to generate the same martensite depth. Moreover, the thickness change of the martensite layer is more sensitive to the change of the input heat flux when $w = 0$ (Fig. 10(b)). Compared with the residual stresses associated with a low table speed (e.g. Pe = 1), a high table speed (e.g. Pe = 4) would increase slightly the maximum surface residual stresses if phase change occurs. This is attributed to the higher yield stress of martensite associated with a higher Pe and a larger H, as indicated by Fig. 11.

The effect of grinding conditions on the nature of residual stresses can be understood more deeply by comparing the influence of the causes individually and with different combinations. Fig. 12 shows the role of each mechanism of different grinding conditions on the longitudinal residual stress, σ_{xx}. Under sole mechanical conditions (case 1), a very small, almost negligible, residual stress is developed. Sole thermal grinding conditions without surface hardening (case 2) lead to a tensile residual stress, which decreases gently with the subsurface depth. When the phase transformation (surface hardening) is coupled, see case 3 however, a surface layer with a greater
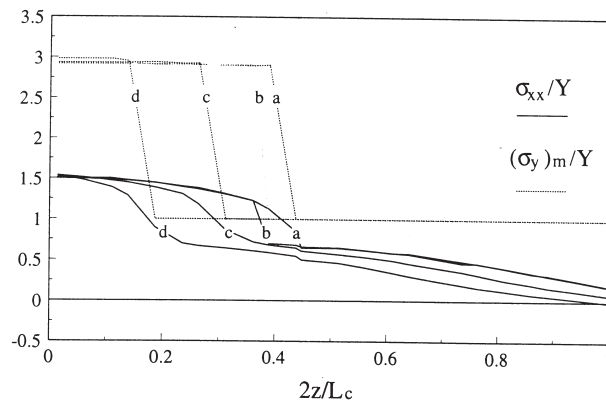

Fig. 9.   Martensite yield stress, σ_y, and the residual stress in grinding direction, σ_{xx} ($H = 0$, Pe = 1, $p_a = 0$). Curve a: $l_a = 0.25$, $q_a = 80$ MW/m². Curve b: $l_a = 0.25$, $q_a = 70$ MW/m². Curve c: $l_a = 0.25$, $q_a = 60$ MW/m². Curve d: $l_a = 0.75$, $q_a = 70$ MW/m².

a

σ_{xx}/Y
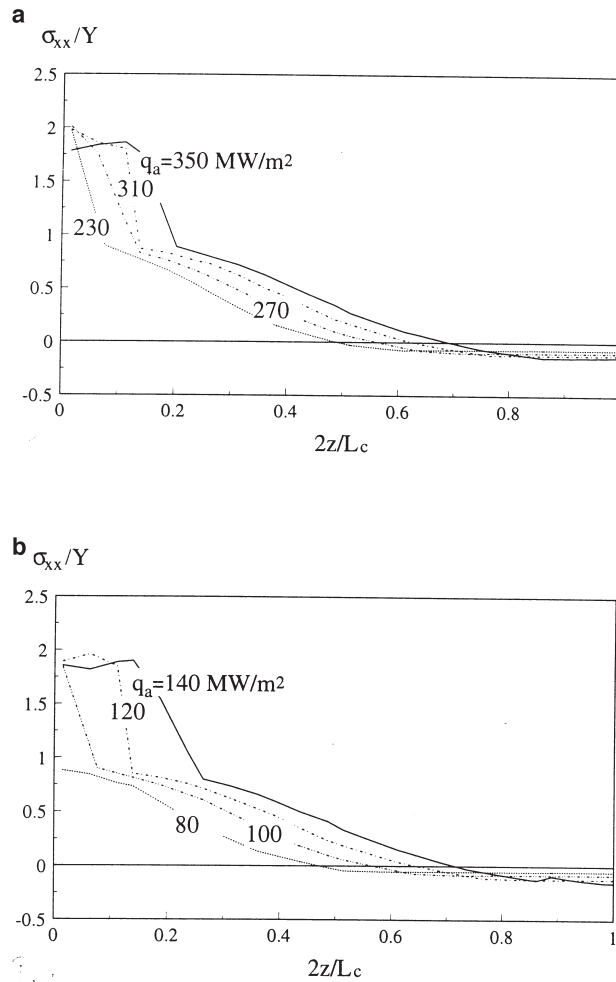

$2z/L_c$

b σ_{xx}/Y

$2z/L_c$

Fig. 10.   The effect of cooling on thermal residual stresses ($l_a = 0.25$, $H = 0$ and Pe $= 4$); (a) $w = 1$, (b) $w = 0$.

tensile residual stress is generated. The variation of σ_{xx} also becomes sharper compared with case 2. By coupling the mechanical grinding conditions of case 1 with those of case 3, a considerable decrease in residual stress occurs, see case 4. It means that mechanical grinding conditions may have stronger effects on residual stresses when combined with thermal conditions only, particularly at a lower Pe. This is similar to the results of thermo-mechanical grinding conditions when the work material properties are temperature-independent [8].

4. Conclusions

A comprehensive analysis of residual stresses induced by surface grinding has been conducted with the aid of the finite element method. The influence of the full coupling of all the three
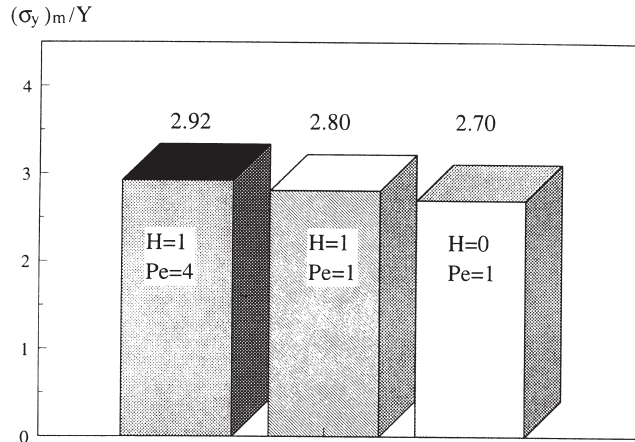
$(\sigma_y)_m/Y$

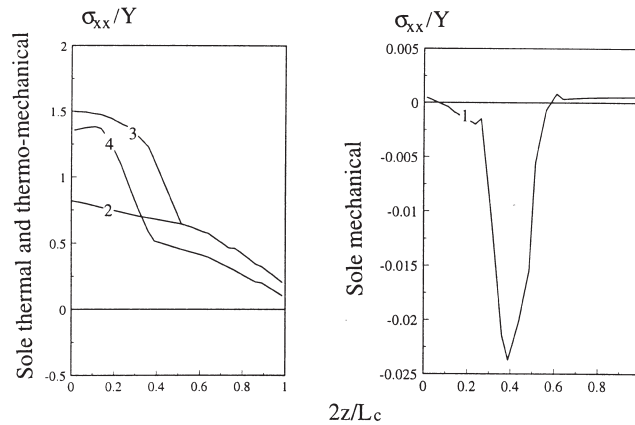Fig. 11.   Martensite yield stresses ($l_a = 0.25$, $T_{max} = T_{aust}$).

Fig. 12.   Effect of individual grinding conditions. Case 1: $P_a/Y = 2.0$, $\mu = 0.1$. Case 2: $q_a = 80$ MW/m^2, Pe = 1, $H = 0$. Case 3: Case 2 coupled with phase transformation. Case 4: Case 3 coupled with Case 1.

sources of deformation has been investigated carefully in terms of thermal and mechanical grinding variables.

To model the property change of work materials due to phase change, a special user-supplied code has been developed successfully. The study concludes

1. that the surface hardening associated with phase change is slightly increased if cooling is more effective,
2. that the influence of mechanical grinding conditions on residual stress distribution is minor when phase change takes place,
3. that all the components of surface residual stresses become tensile when phase transformation occurs, which is independent of the cooling conditions and type of grinding operations, and
4. that the distribution of the residual stress in grinding direction is nearly linear in both the

martensite and non-martensite zones, but the location of the maximum residual stress is related to the depth of martensite and surface mechanical loads.

Acknowledgements

References

[1] L. Zhang, T. Suto, H. Noguchi, T. Waida, An overview of applied mechanics in grinding, Manufacturing Review 5 (1992) 261–273.

[2] M. Mahdi, L. Zhang, Correlation between grinding conditions and phase transformation of an alloy steel, in: L.C. Wrobel et al. (Eds.), Advanced Computational Methods in Heat Transfer III, Computational Mechanics Publications, Southampton, 1994, pp. 193–200.

[3] M. Mahdi, L. Zhang, The finite element thermal analysis of grinding processes by ADINA, Computer and Structure 56 (1995) 313–320.

[4] L. Zhang, M. Mahdi, Applied mechanics in grinding, Part IV: the mechanism of grinding induced phase transformation, International Journal of Machine Tools and Manufacture 35 (1995) 1397–1409.

[5] M. Mahdi, L. Zhang, A theoretical investigation on the mechanically induced residual stresses due to surface grinding, in: N. Narutaki et al. (Eds.), Progress of Cutting and Grinding, vol. III, Japan Society for Precision Engineering, Osaka, 1994, pp. 484–487.

[6] M. Mahdi, L. Zhang, Applied mechanics in grinding, Part V: thermal residual stresses, International Journal of Machine Tools and Manufacture 37 (1997) 619–633.

[7] M. Mahdi, L. Zhang, Applied mechanics in grinding, Part VI: residual stresses and surface hardening by coupled thermo-plasticity and phase transformation, International Journal of Machine Tools and Manufacture 38 (1998) 1289–1340.

[8] M. Mahdi, L. Zhang, Residual stresses in ground components: effect of thermo-mechanical deformation, in: D. Chen et al. (Eds.), Proceedings of the 4th International Conference on Progress of Cutting and Grinding, International Academic Publishers, Beijing, 1998, pp. 447–452.

[9] ADINA R&D Inc., Theory and Modelling Guide, Report ARD 92-5, ADINA R&D Inc., December, 1992.

[10] K.-J. Bathe, Finite Element Procedures in Engineering Analysis, Prentice Hall, New Jersey, 1982.